*mining*

MDPI

*Article*

# From Subsidence to Uplift in the Kłodawa Salt Mine: A Zero-Vertical-Velocity Zone Linked to Deep Convergence

**Jakub Pietras [1], Damian Kurdek [2], Ryszard Hejmanowski [3] and Agnieszka A. Malinowska [3,*]**

[1] Research and Development Centre for Mining of Chemical Raw Materials "CHEMKOP" sp. z o.o., ul. J. Wybickiego 7, 31-261 Krakow, Poland; pietras@agh.edu.pl
[2] Surveying Department, Salt Mine "Kłodawa" S.A., Aleja 1000-lecia 2, 62-650 Kłodawa, Poland
[3] Faculty of Geo-Data Science, Geodesy and Environmental Engineering, AGH University of Krakow, al. A. Mickiewicza 30, 30-059 Krakow, Poland
* Correspondence: amalin@agh.edu.pl; Tel.: +48-12-617-45-02

**Abstract**

Rock-salt mines deform through chamber closure and vertical translation of the surrounding rock mass, yet these responses are commonly evaluated separately. This study integrates underground levelling, convergence monitoring, and mine geometry to identify the depth at which vertical motion changes from subsidence to uplift in the Kłodawa Salt Mine, Poland. The database comprises levelling campaigns conducted between 1962 and 2021 and 337 convergence series containing 7671 observations. Annual vertical velocities were calculated between actual survey epochs. The zero-vertical-velocity zone (ZVVZ) was estimated between adjacent measured levels with opposite median velocities; bootstrap resampling and mutual-nearest benchmark pairing quantified sampling uncertainty and local consistency. No transition was bracketed within the monitored 450–630 m interval in 1987–1992. In 1992–1994, shallow levels continued to subside while deeper levels uplifted, yielding crossing depths of 570.4 m in Field 1, 514.4 m in Field 2, and 476.8 m in Field 3. Field 1 retained the reversal in the 1994–2021 average, with a crossing near 585.3 m, although that long interval cannot resolve intermediate changes. Independent, mostly later convergence records show a marked increase in closure below 690 m and increasing horizontal dominance with depth. The ZVVZ is therefore a spatially variable kinematic boundary within a mining-modified deformation field, not a strain-free horizon: roof descent and floor uplift may generate rapid closure while mean vertical translation remains near zero. The method provides a reproducible monitoring state for deep salt mines. Future work should re-adjust the historical levelling networks, acquire synchronous levelling and convergence data at 690–780 m, and test excavation, geology, and backfilling controls using a calibrated three-dimensional viscoplastic model.

**Keywords:** rock salt; underground mining; mining geodesy; levelling; convergence; floor heave; deformation monitoring; zero-vertical-velocity zone

Check for updates

Academic Editor: Vasyl Lozynskyi

Received: 1 August 2026
Revised: 2 September 2026
Accepted: 8 September 2026
Published: 10 September 2026

**Copyright:** © 2026 by the authors. Licensee MDPI, Basel, Switzerland. This article is an open access article distributed under the terms and conditions of the Creative Commons Attribution (CC BY) license.

## 1. Introduction

Rock salt exhibits time-dependent creep under sustained deviatoric stress, so underground openings continue to deform long after excavation. Deformation rate and mode depend on stress, temperature, loading history, and the active creep mechanism [1–3]. Although increasing depth generally raises the stress acting around an opening, the response is also controlled by excavation geometry, non-salt interbeds, excavation-induced damage, and constitutive behaviour [4–7]. Laboratory and numerical studies further demonstrate

that transient, steady-state, and tertiary creep represent distinct stages and should not be treated as a single process [8,9].

Interpretation also depends on the measured quantity. Convergence represents shortening of a roof–floor or wall–wall baseline, whereas levelling records vertical translation of individual benchmarks within a survey network. Consequently, a chamber may close rapidly while its mean elevation changes only slightly, for example, when roof descent and floor uplift are of comparable magnitude. Damage and dilatancy may further modify the local response [10,11]. Reliable interpretation therefore requires chamber closure to be distinguished from benchmark translation.

Most field investigations capture only one component of this coupled system. Repeated lidar has resolved local closure in a salt gallery and supported rheological calibration [12], while levelling, GNSS, and InSAR have mapped surface deformation above deep salt extraction [13]. Satellite studies have also identified extraction-related sinkholes, regional diapir movement, and adjacent zones of surface uplift and subsidence [14–17]. These findings demonstrate that opposite movement signs can coexist, but they do not locate the depth at which the sign changes inside a multi-level mine.

The Kłodawa Salt Mine provides a rare setting in which this internal transition can be examined. The Zechstein salt structure is strongly folded and contains halite, potash-rich units, anhydrite, and other interbeds [18], with spatially variable mechanical properties [19]. Previous studies documented simultaneous roof lowering and floor heave in an individual chamber, characteristic convergence at great depth, site-scale deformation, and advances in monitoring methods [20–24]. Backfilling is an additional potential control because its stiffness, extent, and age can redistribute load and influence the long-term interaction between excavated voids and creeping salt; international experience therefore identifies backfill performance as an important component of deformation and subsidence control [25]. At Kłodawa, however, the year-by-year backfilling record is not yet sufficiently complete for causal attribution.

Despite these advances, the available literature leaves three linked gaps: the internal depth at which vertical movement changes from subsidence to uplift has not been located; the uncertainty and local spatial consistency of that depth have not been quantified; and levelling-derived translation has rarely been interpreted together with convergence-derived closure. Resolving these gaps is necessary to represent multi-level salt-mine deformation as a coherent vertical system rather than as disconnected monitoring records.

The internal transition is termed the zero-vertical-velocity zone (ZVVZ). This designation is strictly kinematic: it does not denote a geological contact, a plane of zero stress, or a strain-free horizon, but the depth band in which measured vertical velocity changes sign. A stress-reversal surface has been described theoretically in moving salt sheets [26], whereas the ZVVZ defined here is derived directly from mine-survey observations and refers to benchmark translation.

Accordingly, the analysis addresses four questions: (1) whether exact-epoch levelling reveals a repeatable change from subsidence at shallow levels to uplift at greater depth; (2) whether the transition occurs at the same depth in different mining fields; (3) whether local benchmark pairs support the field-scale estimates under alternative pairing distances; and (4) whether the deeper mine is characterised by stronger and more directional convergence. By integrating these elements, the study provides a reproducible basis for identifying vertically partitioned deformation, prioritising resurvey levels, evaluating mining and backfilling controls, and defining uncertainty-aware state variables for a future predictive mine model. The current implementation is explicitly diagnostic rather than predictive [27,28].

## 2. Materials and Methods

### *2.1. Geological and Mining Setting*

The Kłodawa Salt Mine exploits an Upper Permian Zechstein salt structure in central Poland. Competence contrasts and repeated salt flow have produced heterogeneous folding, sheath folds, and subordinate diapiric forms [18]. Studies of impure salt further show that rheological layering can guide long-term strain localisation and folding [29]. The mine contains vertically stacked chamber-and-pillar workings in several fields; Fields 1, 2, and 3 were selected because they provide the most complete overlap between historical levelling and convergence records.

The analysed workings extend from the nominal 450 m level to the 780 m level. The harmonised geometry contains 838 chamber polygons at 450–660 m and 714 generalised outlines at 690–780 m. Because extraction progressed downward, the early observations represent a shallower mining configuration than the later observations. Consequently, the absence of uplift during an early interval may indicate either that a deep uplift regime had not yet developed or that it lay below the levels then monitored; the available record cannot fully distinguish between these explanations.

### *2.2. Monitoring Record*

Table 1 summarises the monitoring archive and its analytical role. The convergence archive contains 337 series and 7671 observations. Quality screening preceded rate calculation: records lacking valid dates, usable baseline lengths, documented metric units, or positive observation intervals were excluded from quantitative analysis, and unsupported absolute rates above 50 mm $yr^{-1}$ were rejected. P1 and P2 series have documented metric baselines and were retained for closure analysis. The P3/P5 subset contains 76 series and 937 observations, but its source unit is not recorded consistently; these records remain available for qualitative screening and in the Supplementary Materials but are not combined with P1/P2 in mm $yr^{-1}$. Complete instrument-calibration histories are not available for the entire historical archive, so instrument-specific corrections could not be reconstructed uniformly.

**Table 1.** Monitoring and spatial data used in this study.

| Data Source | Available Record | Coverage | Role in This Paper |
|---|---|---|---|
| Convergence P1 | 79 series; 3030 observations | 3 August 1978 to 1 July 2025; median span: 19.5 yr | Metric closure analysis |
| Convergence P2 | 182 series; 3704 observations | 9 October 1980 to 16 November 2023; median span: 12.9 yr | Metric closure and deep-level analysis |
| Convergence P3/P5 | 76 series; 937 observations | 31 December 2003 to 31 December 2025; median span: 8.0 yr | Included in the Supplementary Materials only; source unit not confirmed |
| Underground levelling | 1242 station records; 1115 usable geometries | Levels: 450–630 m; key epochs: 1987, 1992, 1994, and 2021 | Vertical profiles and zero-vertical-velocity zone (ZVVZ) |
| Surface levelling | 329 station records; 295 usable geometries | Context interval: 1992–1999 | Far-field-movement sign only |
| Excavation geometry | 838 chamber polygons; 714 deep-level outlines | Levels: 450–780 m | Spatial matching and map context |
| Geology and infrastructure | Level geology, contacts, salt top, shafts, water, and hazards | Multi-level spatial database | Context and future control analysis |

The underground levelling database contains 1242 station records, including 1115 with usable geometry. Survey epochs are available for 1962, 1980, 1981, 1983, 1985, 1987, 1992, 1994, and 2021, with the most complete common coverage between 450 and 630 m. Actual consecutive survey intervals were analysed: 1987–1992 represents the preceding regime, 1992–1994 provides the clearest common comparison across three fields, and 1994–2021 is retained as a single 27-year average only to assess long-term persistence. Surface levelling from 1992 to 1999 provides the far-field-movement sign but is not synchronous with the principal underground interval.

### *2.3. Integrated Spatial Data Model*

All source layers were inventoried, checked, and harmonised in a GeoPackage-based model in EPSG:2180. Common identifiers link mining fields, chambers, convergence centres, benchmarks, survey epochs, geological units, and infrastructure. Original values, units, file names, provenance, and quality flags were retained so that every derived result can be traced to its source and quality-control decision.

Figure 1 summarises the spatial framework and the non-uniform monitoring coverage. Unequal station density can weight a field median toward intensively surveyed corridors, missing levels can prevent a sign bracket from being identified, and sparse local pairs limit lateral validation. These effects were reduced by stratifying the analysis by field and level, reporting medians and bootstrap intervals, and using mutual-nearest benchmark pairs as an independent check. The local constraints follow monitored corridors and do not justify interpolation of a continuous mine-wide ZVVZ surface.

The integrated database is the analytical platform rather than the principal scientific result. Its current maturity is that of a campaign-based descriptive–diagnostic monitoring framework: it stores geometry and monitoring history, applies reproducible quality control, and derives uncertainty-aware diagnostic variables. Figure 2 separates this implemented stage from a predictive digital twin, which would additionally require scheduled data assimilation, calibration of a three-dimensional viscoplastic model, formal uncertainty propagation, and agreed operational response thresholds.

### *2.4. Comparable Survey Intervals and Vertical Velocities*

For benchmark i observed at two actual survey epochs, t1 and t2, the annual vertical velocity was calculated using Equation (1):

$$v_z,i = 1000\,[H_i(t_2) - H_i(t_1)]/\Delta t \quad (1)$$

In Equation (1), H_i(t) is the benchmark elevation adopted from the archived network solution, and $\Delta t$ is the exact elapsed interval in decimal years. Any corrections applied during the original survey processing are therefore embedded in H_i(t). Complete raw readings, atmospheric-refraction logs, rod-calibration records, and instrument histories were not available for every historical epoch, and no additional uniform correction was imposed. The result v_z is reported in mm $yr^{-1}$; positive values denote uplift and negative values denote subsidence. Residual network and datum uncertainty is evaluated separately in Section 2.7.

Only benchmarks with numerical elevations at both epochs and usable geometry were included. Missing coordinates and placeholders were excluded from spatial pairing, while rates with $|v_z| > 50$ mm $yr^{-1}$ were retained only when independently supported. The final 1992–1994 underground layer contains 745 valid stations. For cartographic display, $|v_z| \leq 1$ mm $yr^{-1}$ is classified as near zero to prevent over-interpretation of very small annualised motions. This $\pm 1$ mm $yr^{-1}$ band is an operational visual tolerance rather than a statistical detection limit; the ZVVZ calculation and inferential tests use the original signed

velocities without recoding them as zero. Field profiles are summarised by medians and interquartile ranges to reduce sensitivity to local outliers and unequal station counts.

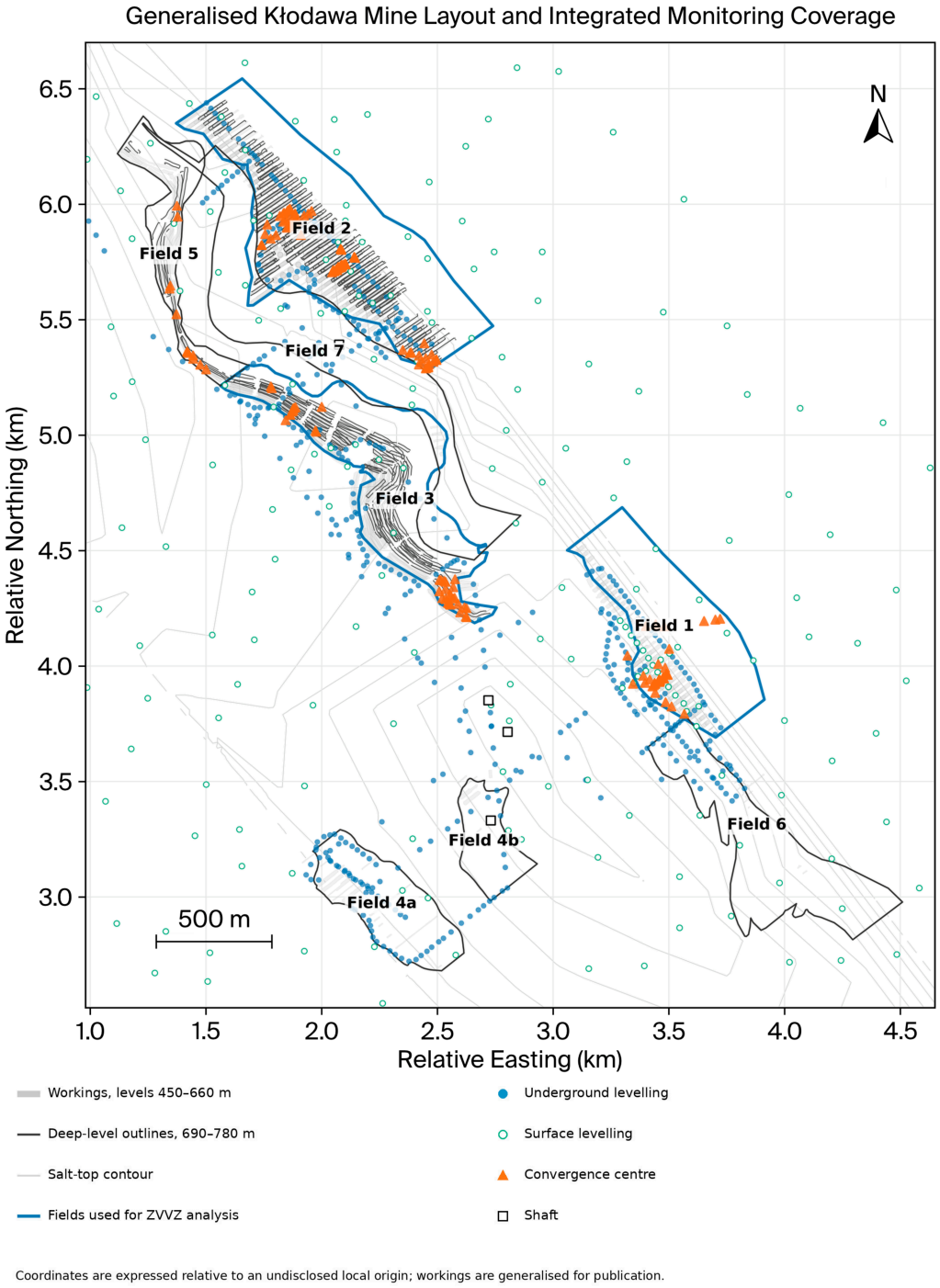



**Figure 1.** Generalised mine layout and integrated monitoring coverage. The map combines mining fields, workings, salt-top contours, shafts, underground and surface levelling stations, convergence centres, and local zero-vertical-velocity zone (ZVVZ) constraints. Relative coordinates and generalised workings protect operational information. The distribution of observations identifies both areas of data overlap and sectors in which the transition remains weakly constrained.

Survey intervals were not forced to a common duration; each displacement was divided by its actual elapsed time. The 1987–1992 and 1992–1994 periods can therefore be compared as annual rates, although their different durations remain relevant when interpreting short-term variability. The 1994–2021 value is a 27-year average and may conceal

one or more intermediate reversals, accelerations, or periods of stability; it establishes only the net sign and average rate between its endpoints. Surface rates from 1992 to 1999 are used solely as non-synchronous context for continued surface subsidence.

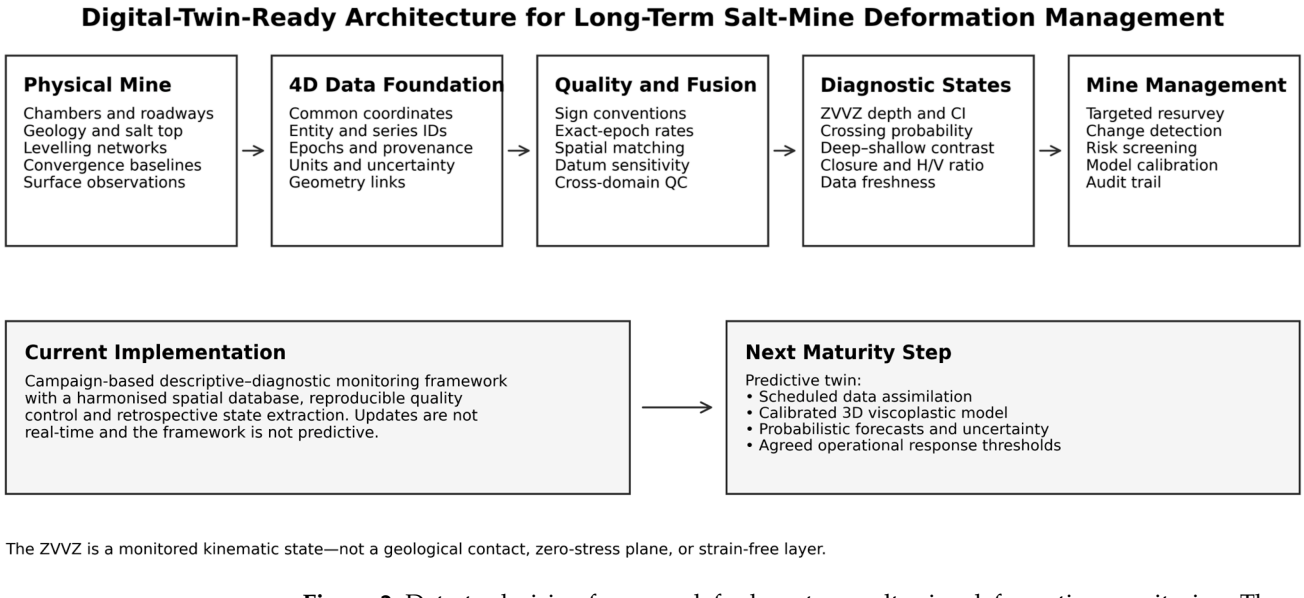



**Figure 2.** Data-to-decision framework for long-term salt-mine deformation monitoring. The upper pathway links physical observations, four-dimensional data management and quality control, diagnostic states, and management use. The lower pathway distinguishes the current campaign-based descriptive–diagnostic monitoring framework from the additional steps required for a predictive digital twin. The ZVVZ is treated as a kinematic monitoring state, not as a geological contact, zero-stress plane, or strain-free layer.

### *2.5. Estimating the Zero-Vertical-Velocity Zone*

Within each field, monitored levels were ordered from shallow to deep. The first adjacent pair with a negative median velocity at the shallower level and a positive median velocity at the deeper level was taken to bracket the transition. If the level depths are z_u and z_l and the corresponding median velocities are v_u and v_l, the crossing depth z_0 is estimated by Equation (2):

$$z_0 = z_u + [-v_u/(v_l - v_u)]\,(z_l - z_u) \quad (2)$$

Equation (2) performs linear interpolation only within the two measured levels of opposite sign; it does not assume that the complete velocity profile is linear or that the same gradient continues outside the bracket. Sampling uncertainty was quantified with 50,000 bootstrap resamples. A crossing was retained only when a resample preserved $v_u < 0$ and $v_l > 0$. The 2.5th and 97.5th percentiles define the reported 95% interval, while the proportion of all resamples that retained the sign bracket is reported as a separate robustness measure.

### *2.6. Local Benchmark-Pair Validation*

Because field medians can conceal lateral heterogeneity, benchmarks on adjacent levels were paired using a mutual-nearest-neighbour rule in plan. Maximum plan distances of 5, 10, 20, and 30 m were tested to quantify sensitivity to spatial tolerance and to prevent one station from being reused in several pairs. The field-profile estimate remains the primary result; local pairs provide an independent spatial consistency test rather than a replacement for the field-level profile.

The 1992–1994 dataset produced 238 adjacent-level pairs, of which 52 changed from subsidence at the shallower station to uplift at the deeper station. The principal validation used the same level brackets as the field profiles: 525–600 m in Field 1, 500–525 m in Field 2, and 450–525 m in Field 3. These brackets contain 36 pairs, including 23 direct sign crossings.

For each principal pair, the deeper-minus-shallower velocity contrast was calculated using Equation (3):

$$\Delta v = v_l - v_u \quad (3)$$

A one-sided exact binomial test assessed whether more than half of the contrasts were positive, and a one-sided Wilcoxon signed-rank test assessed whether the contrast distribution exceeded zero. When a pair changed from negative to positive velocity, a local z_0 value was calculated using the same within-bracket interpolation.

### *2.7. Sensitivity to a Common Vertical Datum Shift*

Historical network adjustment may introduce a common velocity offset for all benchmarks within one field and survey interval. The observed velocity can therefore be written as Equation (4):

$$v_obs = v_true + \delta \quad (4)$$

where $\delta$ is the common offset. Because the same $\delta$ is added to both levels, the deeper-minus-shallower contrast is unchanged, as shown in Equation (5):

$$(v_l + \delta) - (v_u + \delta) = v_l - v_u \quad (5)$$

A spatially uniform offset can change the numerical depth of z_0 but cannot remove a positive deeper-minus-shallower gradient. Accordingly, the range of $\delta$ values that preserves a negative shallow median and a positive deep median was calculated for each field. This test does not establish datum stability. A non-uniform shift—such as field-specific, level-specific, or locally distorted network adjustment—would not cancel in Equation (5) and could alter both the gradient and the sign bracket. Absolute ZVVZ depths must therefore remain provisional until the original networks are re-adjusted consistently.

### *2.8. Convergence Processing and Depth Comparison*

Convergence was derived from dated baseline lengths, with negative signed rates denoting shortening. Intervals shorter than 30 days, records without documented metric baselines, and unsupported absolute rates above 50 mm $yr^{-1}$ were excluded from quantitative analysis. Series-level behaviour was represented by robust medians and Theil–Sen slopes, with recent observations used when a sufficient number of accepted intervals was available. Closure speed is reported as the positive magnitude of shortening. This procedure limits the influence of short-interval noise and accommodates the non-linear, history-dependent deformation of salt [2,8,12,24].

The deep comparison uses P2 horizontal and vertical series in Field 2 at 660, 690, 720, 750, and 780 m. Level medians and 10th–90th percentiles describe the distributions. For co-located centres, H/V is defined as horizontal closure divided by vertical closure; H/V > 1 denotes horizontal dominance. The 780 m result is exploratory because each direction is represented by one centre observed for approximately 0.92 years. Most deep convergence records post-date the 1992–1994 levelling interval, and later mining or deepening may itself increase closure. Treating these records as synchronous validation would therefore risk attributing a temporal change to depth. They are used only as independent evidence of the later deep deformation regime, not as proof of a contemporaneous cause.

### *2.9. Interpretation and Reporting Rules*

Direct results are restricted to the measured sign change, the positive deeper-minus-shallower gradient, their sampling uncertainty, and the observed convergence distributions. Progressive mining depth, interactions among stacked workings, creep, geology, and backfilling are plausible controls, but causal attribution requires a validated annual extraction and backfilling history. Similarly, the absence of an early crossing means only that no sign reversal was bracketed within the levels then observed.

For monitoring, the database stores z_0, its bootstrap interval, sign-bracket retention, local crossings, the deeper-minus-shallower contrast, horizontal and vertical closure, H/V, data age, provenance, and quality flags. The available data do not support a universal minimum sampling density or hazard threshold. For implementation at Kłodawa, a provisional reporting rule is proposed: update the ZVVZ after every complete levelling campaign and at least annually in active deep fields, as well as after major extraction or backfilling changes; require at least 10 valid benchmarks on each bracketing level, at least five spatially distributed mutual-nearest local pairs, and $\geq$90% bootstrap sign-bracket retention. Estimates that do not satisfy these criteria should be reported as "insufficiently constrained". These values are survey-design criteria to be calibrated prospectively, not universal safety limits.

## 3. Results

### *3.1. From an All-Subsiding Profile to a Two-Direction Profile*

During 1987–1992, median vertical velocity remained negative throughout the commonly monitored 450–630 m interval in Fields 1–3 (Figure 3). The profile was therefore dominated by downward movement, and no adjacent pair of field medians bracketed a change from subsidence to uplift.

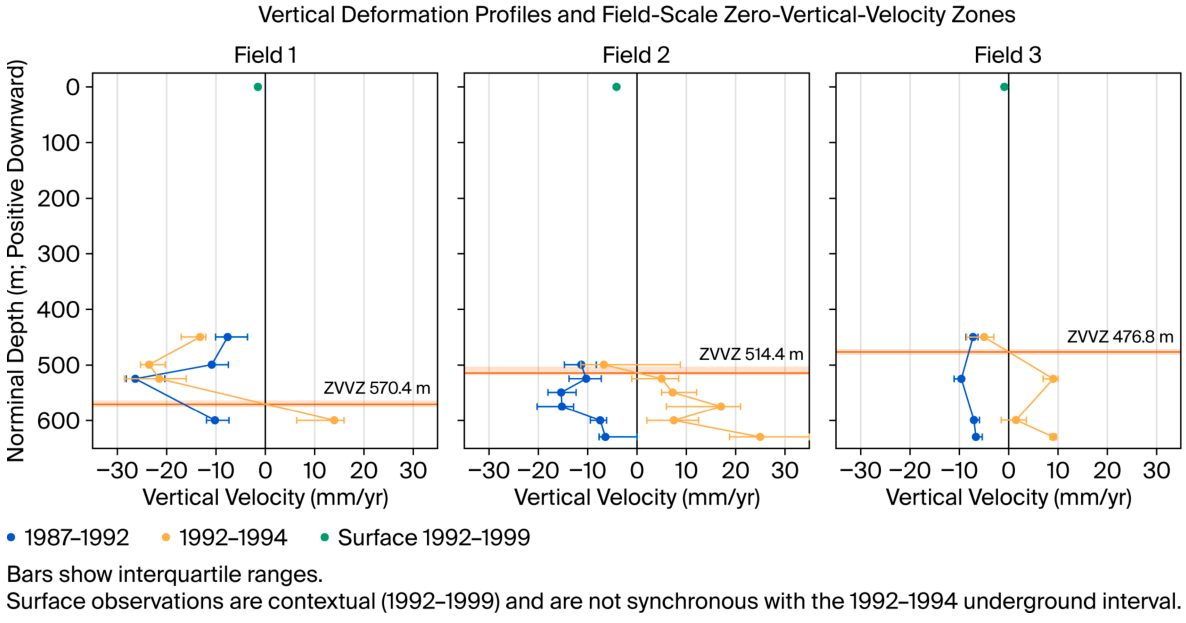



**Figure 3.** Vertical-motion profiles by mining field and survey interval. The horizontal axis progresses from subsidence to uplift, and depth increases downward. Points denote field medians and bars denote interquartile ranges. Horizontal orange lines mark the estimated ZVVZ depths. Surface observations from 1992 to 1999 provide non-synchronous context only.

The pattern changed in 1992–1994: shallow levels continued to move downward, whereas deeper levels moved upward. In Field 1, the median changed from $-21.50$ mm yr$^{-1}$ at 525 m to +14.00 mm yr$^{-1}$ at 600 m. In Field 2, it changed from

−6.75 mm yr$^{-1}$ at 500 m to +5.00 mm yr$^{-1}$ at 525 m and remained positive at the deeper monitored levels. In Field 3, the median changed from −5.00 mm yr$^{-1}$ at 450 m to +9.00 mm yr$^{-1}$ at 525 m. The resulting profile is vertically bidirectional rather than a simple increase in subsidence with depth.

The surface remained within the downward-moving domain over the broader 1992–1999 interval. Median surface rates were −1.52 mm yr$^{-1}$ in Field 1 and −4.16 mm yr$^{-1}$ in Field 2; Field 3 contained only one benchmark within the field polygon, with −0.86 mm yr$^{-1}$. These data support continued surface subsidence but are not synchronous with the 1992–1994 underground interval and cannot be used to calculate a transfer ratio.

Field 1 provides a later persistence test. Over 1994–2021, the 525 m level retained a negative average velocity of −6.67 mm yr$^{-1}$, whereas the 600 m level retained a positive average velocity of +1.63 mm yr$^{-1}$. After exclusion of one sign-inconsistent source value, 42 of 43 stations at 600 m indicated uplift, placing the long-period crossing near 585.3 m. This 27-year average does not reveal whether intermediate reversals occurred. Fields 2 and 3 cannot be assessed equivalently because the intermediate levels needed to bracket a 2021 crossing were not remeasured; their later transitions are unobserved rather than absent.

Figure 4 presents the same transition in map view for Field 1. During 1987–1992, both the 525 and 600 m levels were dominated by negative velocities. A small number of near-zero or locally positive observations occurred at 600 m, but they were sparse and lacked spatial coherence; the level median remained −10.2 mm yr$^{-1}$. During 1992–1994, the 525 m level remained negative, whereas positive velocities became spatially coherent at 600 m. The reversal was therefore a field-scale pattern rather than the effect of a single benchmark.

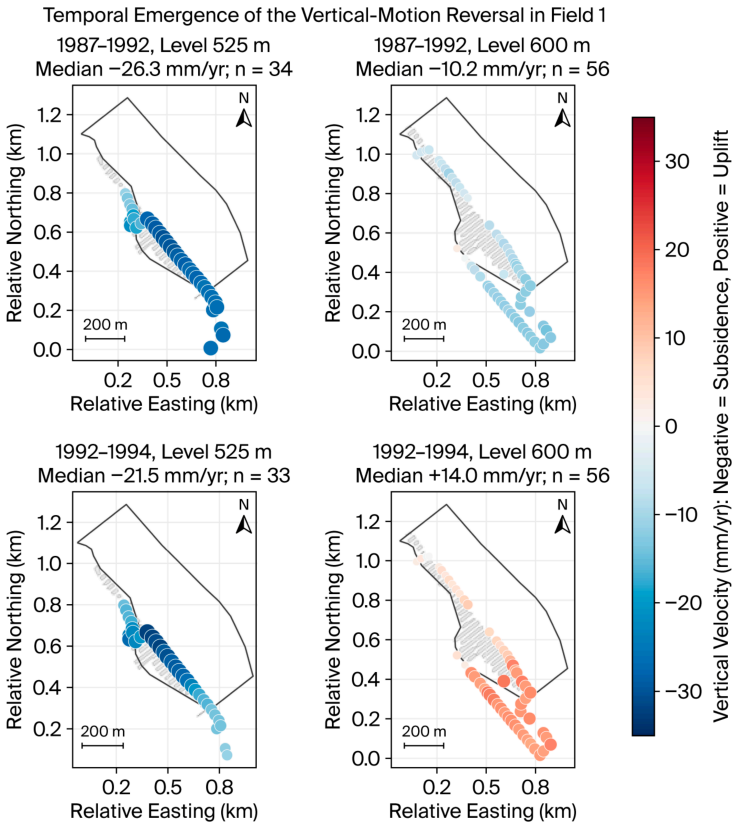



**Figure 4.** Emergence of the vertical-motion reversal in Field 1. The left panels represent 1987–1992 and the right panels represent 1992–1994. Colour denotes annual vertical velocity and symbol size denotes magnitude. Isolated non-negative values at 600 m during 1987–1992 do not alter the negative level median; spatially coherent uplift appears at 600 m only in 1992–1994.

### 3.2. The Transition Depth Differs Between Fields

For 1992–1994, the field-scale estimates place the ZVVZ at 570.4 m in Field 1, 514.4 m in Field 2, and 476.8 m in Field 3 (Table 2). The approximately 94 m range demonstrates that the transition is not a single horizontal plane across the mine.

**Table 2.** Field-scale crossing depths for 1992–1994. Positive vertical velocity denotes uplift; surface rates are provided only as non-synchronous 1992–1999 context.

| Field | Bracketing Levels (m) | Median Velocity, Shallow/Deep (mm Year$^{-1}$) | Stations, Shallow/Deep | ZVVZ Depth (m) | 95% Bootstrap Interval (m) | Bracket Retained (%) | Surface Context (mm Year$^{-1}$) |
|---|---|---|---|---|---|---|---|
| 1 | 525–600 | −21.5/14 | 33/56 | 570.42 | 565.0–575.8 | 100 | −1.52 |
| 2 | 500–525 | −6.75/5 | 40/114 | 514.36 | 504.4–517.2 | 94 | −4.16 |
| 3 | 450–525 | −5/9 | 65/48 | 476.79 | 473.5–480.5 | 100 | −0.86 |

The corresponding 95% bootstrap intervals are 565.0–575.8 m, 504.4–517.2 m, and 473.5–480.5 m. The sign bracket is retained in 100% of resamples for Fields 1 and 3 and in 94% for Field 2. These intervals quantify sampling uncertainty within the observed level brackets but do not include non-uniform datum distortion or unmeasured curvature between levels.

Figure 5 displays the measured levels that bracket each field-scale transition. Within each field, the shallower level has a negative median and the deeper level has a positive median, while individual stations vary around those medians, particularly in Field 2. The ZVVZ is therefore estimated from a population of spatially uneven observations and should not be interpreted as a perfectly uniform layer.

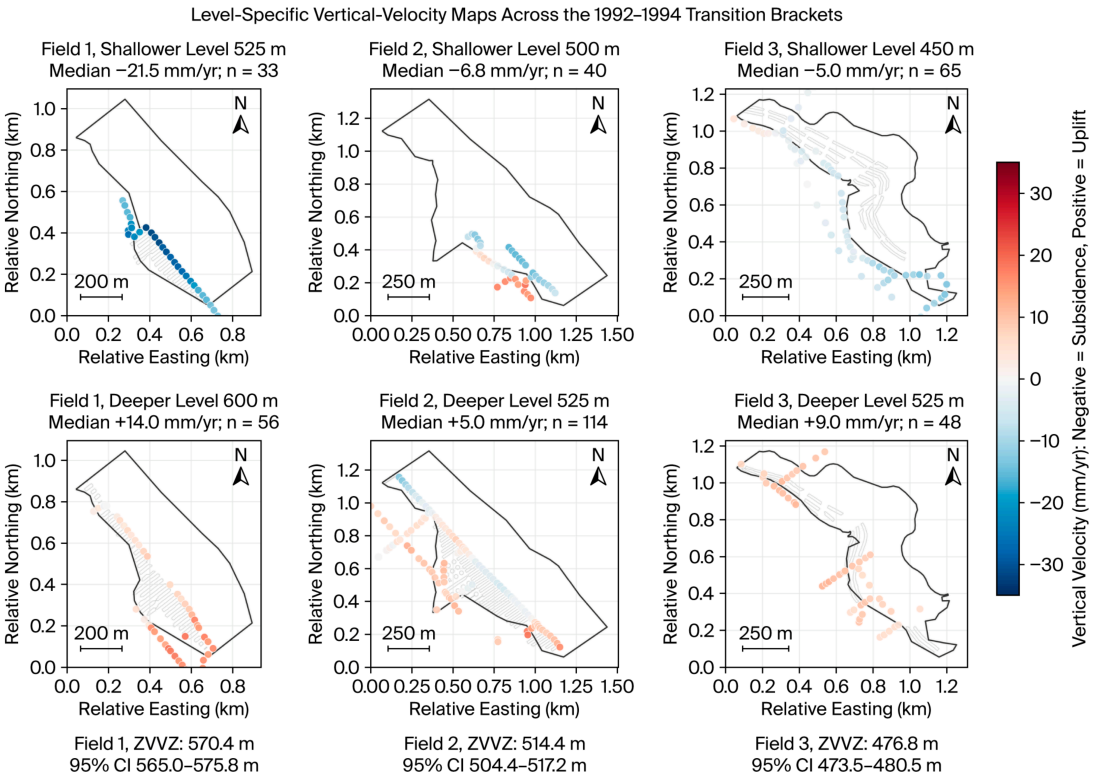



**Figure 5.** Measured levels bracketing the 1992–1994 ZVVZ. Each column represents one field. The upper panel shows the shallower, subsiding level and the lower panel shows the deeper, uplifting level. The field-scale crossing depth and bootstrap interval lie between the measured levels, with no extrapolation outside the bracket.

### *3.3. Local Pairs Support the Field-Scale Pattern*

Across all adjacent-level transitions, 52 mutual-nearest benchmark pairs change from subsidence at the shallower station to uplift at the deeper station (Figure 6). Twenty-three occur within the three primary field brackets. Because the pairs follow monitored corridors, they provide local constraints rather than a continuous surface; their appropriate interpretation is as spatial support for the field-scale depth brackets.

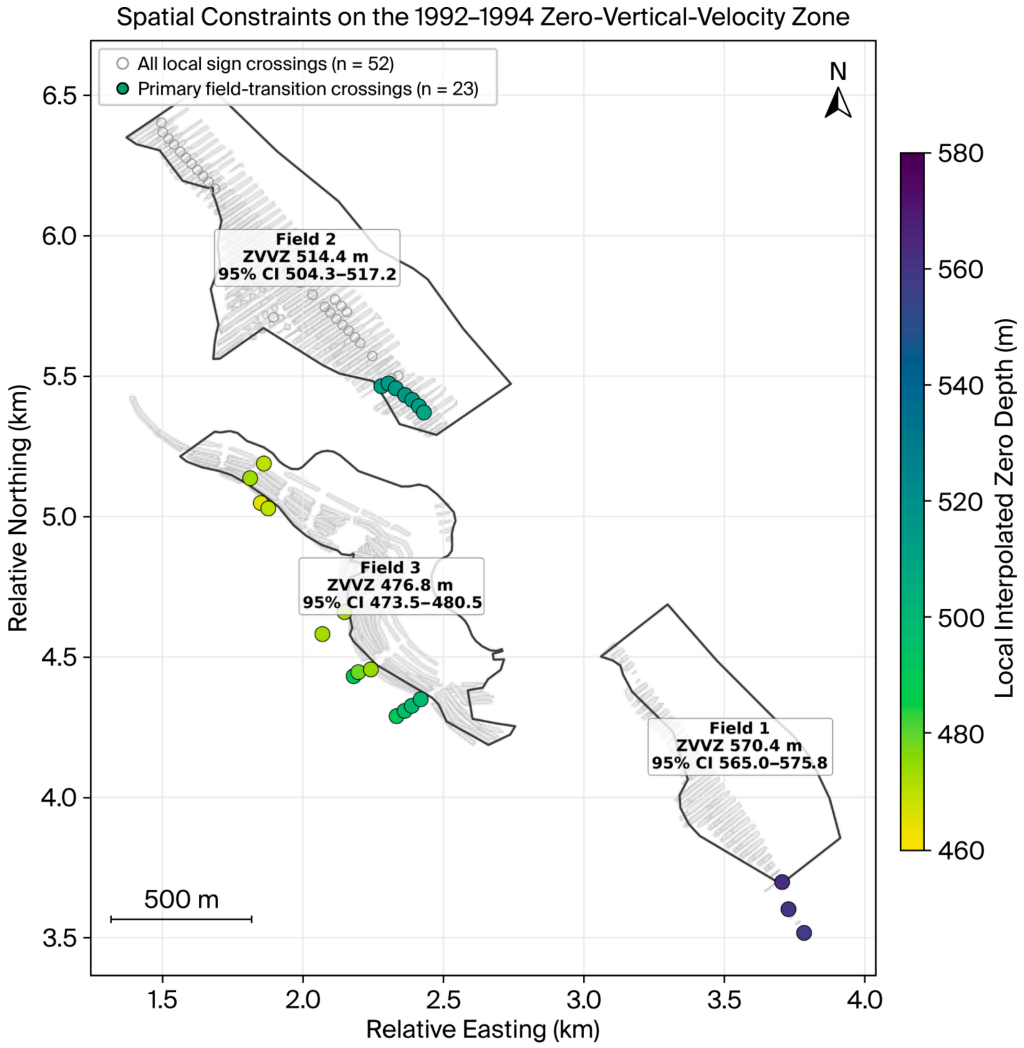



**Figure 6.** Spatial support for the 1992–1994 transition. Grey points represent all 52 local subsidence-to-uplift crossings, and coloured points represent the 23 crossings within the primary field brackets; colour denotes locally interpolated crossing depth. Field labels report the profile estimate and 95% bootstrap interval. Blank areas indicate missing suitable pairs, not necessarily the absence of a transition.

Figure 7 and Table 3 summarise the pairwise evidence. Field 1 contains only three primary pairs; all become more positive at 600 m and all cross from subsidence to uplift. Their median deeper-minus-shallower contrast is +28.0 mm yr$^{-1}$, and local z_0 values range from 557.1 to 562.5 m. The agreement supports the field result, although the sample is too small for strong stand-alone inference.

Field 2 contains 18 primary pairs. Sixteen have a more positive velocity at 525 m than at 500 m, and seven cross zero. The median contrast is +14.0 mm yr$^{-1}$. The exact sign test gives $p = 6.56 \times 10^{-4}$ and the Wilcoxon test gives $p = 2.67 \times 10^{-4}$. The seven local crossings have a median z_0 of 512.8 m, close to the field estimate of 514.4 m.

Field 3 contains 15 primary pairs. All pairs become more positive at 525 m, and 13 cross zero. The median contrast is +13.5 mm yr$^{-1}$. The exact sign test gives $p = 3.05 \times 10^{-5}$ and the Wilcoxon test gives $p = 3.27 \times 10^{-4}$. The local median z_0 is 474.1 m, close to the field estimate of 476.8 m, although the local range is wider.

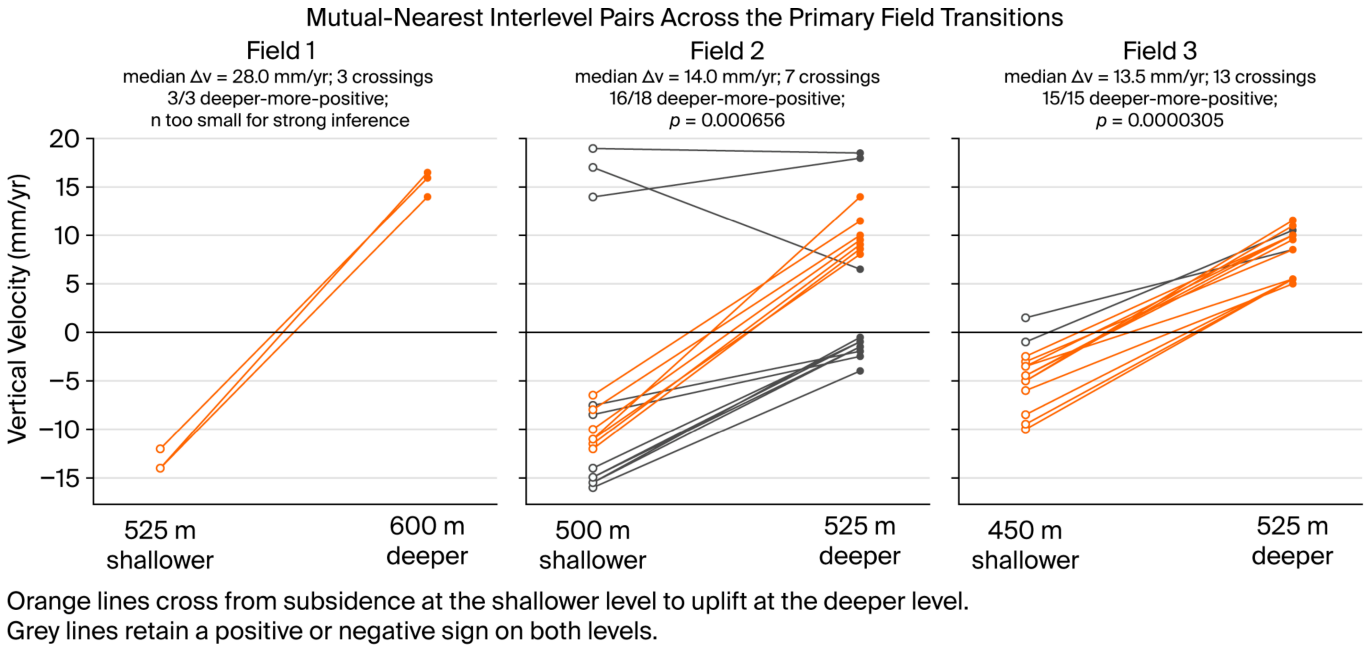



**Figure 7.** Vertical velocities in mutual-nearest benchmark pairs across the primary transitions. Each line connects one shallow and one deep benchmark. Orange lines cross from negative to positive velocity; grey lines retain the same sign at both levels. The original three-field arrangement is retained at full text width to show both the dominant deeper-more-positive tendency and the remaining lateral variability.

**Table 3.** Statistics for mutual-nearest benchmark pairs across the primary field transitions.

| Field | Level Pair (m) | Pairs | Deeper More Positive/ Direct Crossings | Median Contrast (mm Year$^{-1}$) | Sign/Wilcoxon p | Local Crossing Depth, Median (Range), m | Datum-Shift Range Retaining Bracket (mm Year$^{-1}$) |
|---|---|---|---|---|---|---|---|
| 1 | 525–600 | 3 | 3/3/3 | 28.0 | 0.125/0.125 | 559.4 (557.1–562.5) | (−14.00, 21.50) |
| 2 | 500–525 | 18 | 16/18/7 | 14 | $6.56 \times 10^{-4}$/ $2.67 \times 10^{-4}$ | 512.8 (509.0–514.6) | (−5.00, 6.75) |
| 3 | 450–525 | 15 | 15/15/13 | 13.5 | $3.05\times 10^{-5}$/ $3.27\times 10^{-4}$ | 474.1 (465.0–498.4) | (−9.00, 5.00) |

### *3.4. The Depth Gradient Is Robust, but the Absolute Crossing Depends on the Datum*

The field-median deeper-minus-shallower contrast is +35.5 mm yr$^{-1}$ over 75 m in Field 1, +11.75 mm yr$^{-1}$ over 25 m in Field 2, and +14.0 mm yr$^{-1}$ over 75 m in Field 3. These values correspond to positive gradients of 47.3, 47.0, and 18.7 mm yr$^{-1}$ per 100 m, respectively. A spatially uniform datum shift does not change these contrasts.

The absolute negative-to-positive bracket is more sensitive. It is retained for uniform velocity offsets from −14.0 to +21.5 mm yr$^{-1}$ in Field 1, −5.0 to +6.75 mm yr$^{-1}$ in Field 2, and −9.0 to +5.0 mm yr$^{-1}$ in Field 3. Field 2 has the narrowest tolerance. Its deeper-more-positive gradient remains strong, but the crossing depth of 514.4 m should be checked

against a consistent re-adjustment of the original levelling network before being interpreted as an absolute physical surface.

### *3.5. Closure Increases Sharply Below 690 m*

Field 2 provides the clearest deep convergence record (Figures 8 and 9; Table 4). The median horizontal closure is 7.05 mm $yr^{-1}$ at 660 m and 9.38 mm $yr^{-1}$ at 690 m, increasing to 22.83 mm $yr^{-1}$ at 720 m and 34.57 mm $yr^{-1}$ at 750 m. The median vertical closure at the same levels is 4.25, 6.22, 18.89, and 25.26 mm $yr^{-1}$. The larger 780 m values are exploratory because each direction is represented by one short series.

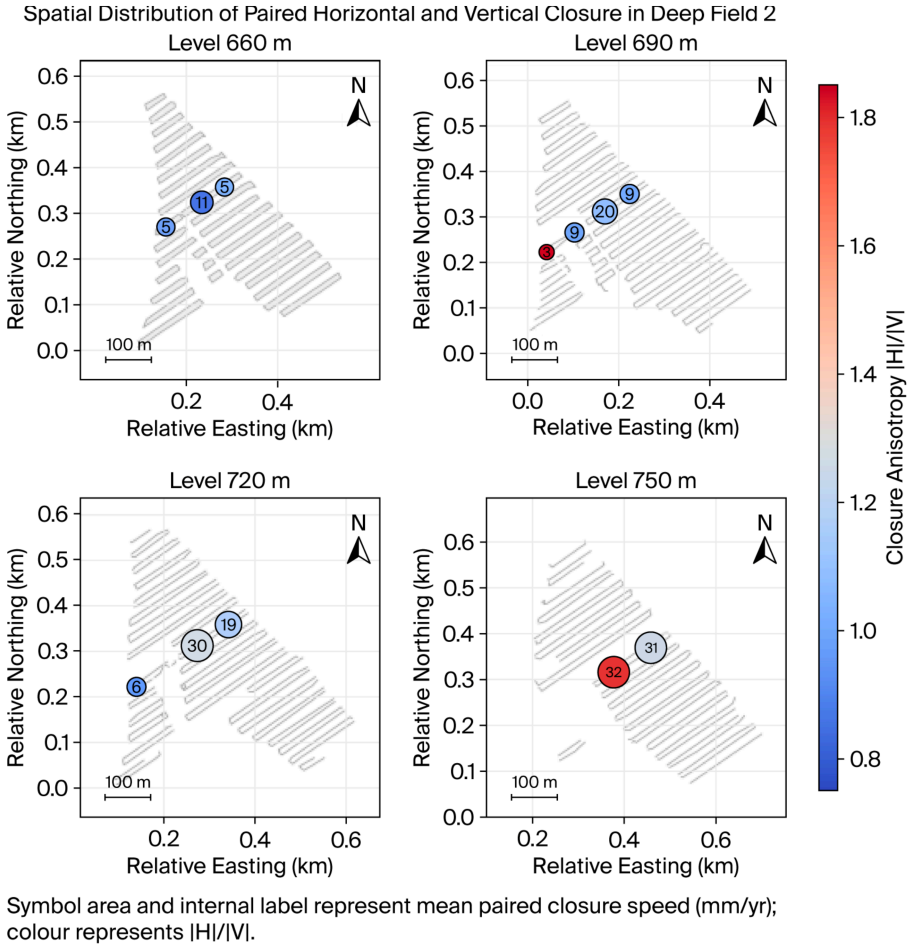



**Figure 8.** Spatial concentration of deep closure in Field 2 at 660, 690, 720, and 750 m. Circle area represents the mean paired closure rate, and the numbers inside the circles give the corresponding values in mm $yr^{-1}$. Colour indicates the horizontal-to-vertical closure ratio ($|H|/|V|$), where H and V denote horizontal and vertical closure rates, respectively. Ratios greater than 1 indicate horizontal dominance, whereas ratios below 1 indicate vertical dominance. Closure is spatially heterogeneous and concentrated in particular chamber groups.

The depth association is stronger for horizontal than for vertical closure: Spearman's ρ is 0.833 for the horizontal direction and 0.447 for the vertical direction. Directional balance also changes, with the median H/V increasing from 0.983 at 660 m to 1.518 at 750 m. Horizontal and vertical closure are therefore approximately balanced at 660 m, whereas horizontal closure is clearly dominant at 750 m.

The increase is not spatially uniform within each level (Figure 8). Larger values occur in specific monitored chamber groups, so the map should be interpreted as a spatial distribution rather than solely as a sequence of level averages.

Large closure at depth does not imply acceleration with calendar time. A repeated-interval model for P2 yields a coefficient of approximately +0.060 mm $yr^{-1}$ per calendar year for the signed rate. Because shortening is negative, the positive coefficient indicates that rates became modestly less negative on average. Deep workings may therefore exhibit high closure magnitudes while individual series stabilise over time.

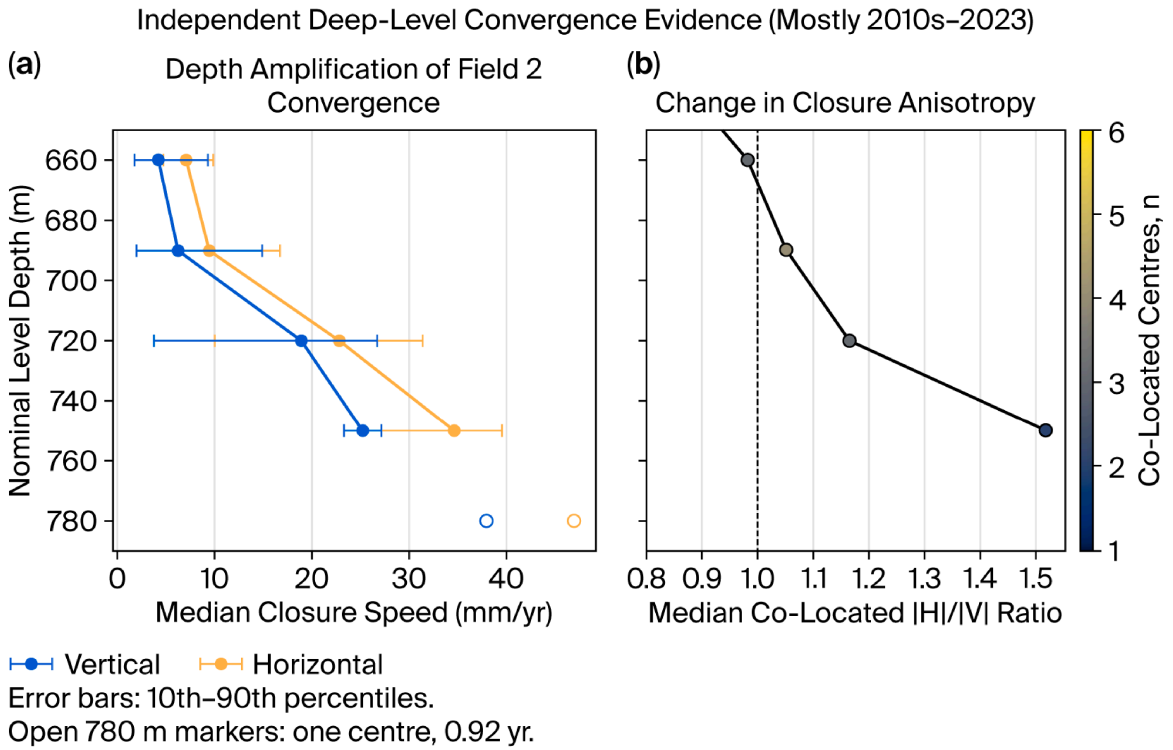



**Figure 9.** Depth dependence of Field 2 convergence. Panel (**a**) compares horizontal and vertical closure, with bars showing the 10th–90th percentile range; panel (**b**) shows median H/V for co-located centres. The dashed vertical line at $|H|/|V| = 1$ denotes equal horizontal and vertical closure rates; values above 1 indicate horizontal dominance, whereas values below 1 indicate vertical dominance. The largest change occurs between 690 and 720 m. Open markers at 780 m are exploratory. Because these records mostly post-date the 1992–1994 levelling interval, they are interpreted as independent later-regime evidence rather than a contemporaneous validation of the ZVVZ.

**Table 4.** Deep Field 2 convergence and horizontal-to-vertical anisotropy.

| Level (m) | Horizontal Series, *n* | Horizontal Closure (mm $Year^{-1}$) | Vertical Series, *n* | Vertical Closure (mm $Year^{-1}$) | Co-Located Pairs, *n* | Median H/V | Evidence Class |
|---|---|---|---|---|---|---|---|
| 660 | 4 | 7.045 | 5 | 4.247 | 3 | 0.983 | Primary |
| 690 | 5 | 9.383 | 6 | 6.221 | 4 | 1.052 | Primary |
| 720 | 4 | 22.826 | 5 | 18.894 | 3 | 1.165 | Primary |
| 750 | 3 | 34.571 | 2 | 25.263 | 2 | 1.518 | Primary |
| 780 | 1 | 46.93 | 1 | 37.934 | - | - | Exploratory |

## 4. Discussion

### *4.1. ZVVZ Distinguishes Vertical Translation from Chamber Closure*

The central result is a vertically partitioned deformation field. During 1992–1994, shallow benchmarks moved downward while deeper benchmarks moved upward, and the transition was independently identified in three fields. The 94 m range in field-scale crossing depths shows that the ZVVZ is spatially variable rather than a single mine-wide horizon. Field 1 additionally retains the bidirectional profile in the 1994–2021 average, although the long interval does not resolve its internal chronology.

The ZVVZ separates the signs of benchmark translation but does not represent zero strain. Roof descent and floor uplift contribute additively to roof–floor convergence even when their mean vertical translation is near zero. This distinction resolves the apparent contradiction between a zero-velocity band and rapid chamber closure and is consistent with earlier chamber-scale observations of floor heave accompanying greater roof lowering at Kłodawa [20].

The principal contribution is therefore methodological as well as descriptive: exact-epoch multi-level levelling, an explicit negative-to-positive bracket, interpolation of z_0, bootstrap uncertainty, local-pair validation, and directional convergence are integrated into one reproducible interpretation. The evidence supports a mining-modified deep-squeeze regime with internal uplift below the transition, but it does not establish natural uplift of the entire diapir. Such a claim would require an external stable datum, synchronous deep and surface observations, coherent uplift over a larger rock volume, and a model separating regional salt flow from excavation-induced creep [14,16].

Figure 10 illustrates the kinematic interpretation. The dominant translation changes from subsidence above the ZVVZ to an uplift or floor-heave component below it, while opposite roof and floor motions can produce substantial closure near zero mean translation. The transition must therefore not be treated as a stable, safe, or strain-free layer.

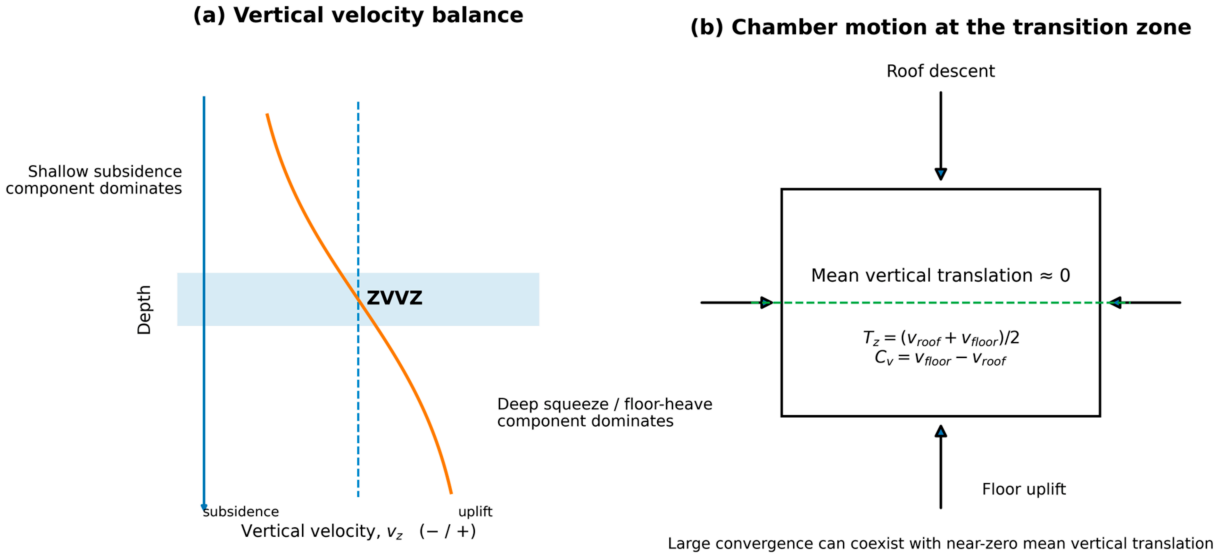



**Figure 10.** Physical interpretation of the ZVVZ. (**a**) Vertical velocity changes from negative above the transition to positive below it; the shaded band represents uncertainty in crossing depth. (**b**) Roof descent and floor uplift may yield near-zero mean vertical translation while producing large roof–floor closure. Zero vertical velocity therefore does not imply zero deformation.

### *4.2. Spatial Variability Reflects Mining, Geological, and Backfilling Controls*

The approximately 94 m difference among field estimates is mechanically plausible because Kłodawa is not a homogeneous salt body. Folding, anhydrite- and potash-rich units,

and spatially variable material properties produce a complex internal structure [18,19], while rheological layering can localise deformation over long timescales even where halite is dominant [29]. Chamber dimensions, level spacing, overlap, excavation age, and interlevel shelves add further spatial variation.

Progressive deepening provides a plausible, but not uniquely demonstrated, mechanical control. Greater depth increases stress around openings, and a growing number of stacked levels strengthens interaction among chambers, pillars, and shelves. In creeping salt, these changes can intensify lateral inflow, roof descent, and floor heave, with geometry, non-salt interbeds, loading path, and constitutive behaviour determining which component dominates [4–9]. Historical failure cases further show that floor response, pillar loading, and surface movement may form one coupled process [30,31].

Backfilling may modify the same stress-transfer system by reducing void volume, supporting excavation boundaries, and changing load redistribution through time. Experience with tailings-based backfill technologies emphasises their relevance to deformation control and sustainable underground construction [25]. The present database contains backfilling information, but its annual completeness and spatial resolution are insufficient to isolate a backfill effect from depth, excavation age, geology, and chamber overlap. Backfilling is therefore treated as a testable control rather than an established cause.

Chronology imposes an additional constraint. No crossing was bracketed within the monitored range in 1987–1992, which may mean either that the deep uplift regime had not yet developed or that it lay below the available observations. The 1992–1994 interval identifies when the reversal became observable, not its initiation date, and the 1994–2021 average is strongly interval-censored. A causal test requires annual histories of the deepest active horizon, extracted volume, excavation age, chamber overlap, and backfilling.

The crossing depth should consequently be represented conceptually as z_0 (x, y, t), not as one fixed mine-wide number. Current observations constrain it at field scale and at selected local crossings but do not define a continuous three-dimensional surface. The observed spatial variation is part of the result rather than noise to be averaged away; assigning a single neutral depth to the whole mine would conceal the influence of local stress, geology, excavation architecture, and monitoring density.

Below approximately 690 m, the later convergence archive records a marked increase in closure and a growing horizontal component. This pattern is consistent with stronger lateral inflow or interaction among stacked openings, but baseline convergence alone cannot determine whether opposing walls move symmetrically or whether the chamber translates. Wall–wall observations should therefore be combined with roof–floor levelling and repeated three-dimensional scanning [12], while closure magnitude, temporal trend, direction, spatial coherence, and uncertainty remain separate decision variables.

### *4.3. Operational Monitoring Criteria and Digital-Twin Integration*

The ZVVZ is useful as an uncertainty-aware monitoring state rather than as a single hazard threshold. It reduces a multi-level velocity profile to a crossing depth, confidence interval, sign-bracket retention, local crossing support, and datum-invariant depth contrast. Combined with horizontal and vertical closure, H/V, data age, provenance, and quality flags, these variables provide a compact description of deformation and evidence strength.

Operational updating should follow each complete levelling campaign, occur at least annually in active deep fields, and be repeated after major extraction or backfilling changes. Because no universal sample-size criterion can be derived from the present archive, the proposed Kłodawa reporting rule is provisional: at least 10 valid benchmarks are required on each bracketing level, at least five mutual-nearest pairs should be distributed across more than one monitored corridor, and bootstrap sign-bracket retention should reach 90%.

Failure to meet these conditions should trigger an "insufficiently constrained" status rather than a numerical ZVVZ used in decisions.

The framework also identifies where additional observations have the highest value. Levels immediately above and below the current bracket are optimal for detecting migration of the transition; areas with high H/V require both wall–wall and roof–floor measurements; and sectors in which field-scale and local estimates disagree require denser control. These principles are transferable to deep salt mines, cavern fields, and storage systems with monitoring distributed across multiple depths.

A functional digital twin must connect incoming observations to interpretable states, update calibrated models, propagate uncertainty, and support decisions [28]. The current Kłodawa implementation remains a campaign-based descriptive–diagnostic monitoring framework rather than a predictive twin. Progression to the predictive stage requires scheduled data assimilation, synchronous deep observations, a calibrated three-dimensional viscoplastic model, probabilistic forecasting, and agreed operational response thresholds [27,32–35].

### *4.4. Causal Attribution Requires Synchronous Monitoring and Model Validation*

The temporal mismatch between levelling and deep convergence is a principal limitation. Most convergence records from 690 to 780 m were acquired after the 1992–1994 levelling interval, when deeper extraction, altered chamber interaction, or changed backfilling conditions may already have modified the deformation regime. The observed increase in closure with depth could therefore partly reflect temporal evolution. It supports the interpretation of a later deep-squeeze regime but cannot validate the contemporaneous mechanism or cause of the 1992–1994 ZVVZ.

Causal proof requires four coordinated steps: (1) re-adjustment of the 1987, 1992, and 1994 levelling networks from original height differences, closure errors, and reference-benchmark histories; (2) extension of absolute levelling or three-dimensional control to 690–780 m so that translation and convergence are observed synchronously; (3) validation of annual extraction depth, excavated volume, overlap, excavation age, and backfilling; and (4) calibration of a three-dimensional viscoplastic model that tests whether these controls reproduce both the sign reversal and its field-specific depths, including constitutive and dilatancy uncertainty [6,9–11]. The P3/P5 source unit must also be confirmed before its 937 observations are combined quantitatively with P1/P2. These limitations affect causal interpretation and absolute crossing depth but do not remove the observed deeper-more-positive gradient.

## 5. Conclusions

Integration of levelling, convergence, and mine geometry provides a coherent vertical description of deformation in the Kłodawa Salt Mine. The principal conclusions are as follows:

1. The monitored profile changed through time. All commonly observed levels subsided in 1987–1992, whereas the 1992–1994 profile combined continued shallow subsidence with uplift at deeper monitored levels.
2. The sign reversal defines a spatially variable ZVVZ. Its 1992–1994 depth was 570.4 m in Field 1, 514.4 m in Field 2, and 476.8 m in Field 3, demonstrating that the transition is not a single horizontal mine-wide layer.
3. Field 1 retains the reversal in the 1994–2021 average, with the 525 m level subsiding and the 600 m level uplifting and a crossing near 585.3 m. The 27-year average may, however, conceal intermediate changes in sign or rate.

4. Local benchmark pairs support the field estimates: 23 primary pairs cross directly from negative velocity above to positive velocity below. The deeper-more-positive gradient is invariant only to a spatially uniform datum offset; non-uniform network adjustments remain a limitation, and absolute ZVVZ depths require re-adjustment of the historical networks.
5. Independent convergence records show a marked increase below 690 m and growing horizontal dominance toward 750 m. Because these observations mostly post-date the 1992–1994 levelling interval, they indicate a later deep deformation regime but do not prove the contemporaneous cause of the ZVVZ.
6. For monitoring, the ZVVZ should be updated after each complete campaign and reported together with its bootstrap interval, sign-bracket retention, local-pair support, datum sensitivity, H/V, and data age. The proposed minimum sampling criteria are provisional survey-design rules and must not be interpreted as universal safety thresholds.
7. Future research should re-adjust the historical levelling networks, establish synchronous translation and convergence monitoring at 690–780 m, validate annual extraction and backfilling histories, and calibrate a three-dimensional viscoplastic model capable of testing the observed reversal and its spatial migration.

The study provides a reproducible method for locating where subsidence changes to uplift, quantifying the uncertainty of that location, and explaining why rapid closure can coexist with near-zero mean vertical velocity. The evidence supports a mining-modified, vertically partitioned deformation field, but it does not yet establish natural uplift of the entire Kłodawa diapir.

**Supplementary Materials:** The following supporting information can be downloaded at https://www.mdpi.com/article/10.3390/mining6030080/s1, Figure S1: Long-period evidence from Field 1 (1994–2021); Figure S2: Geological context, chamber geometry, and monitoring locations at the 600 m level; Figure S3: Chronology of the observed vertical-motion reversal; Table S1: Field- and level-scale vertical-velocity profiles; Table S2: Field-scale neutral-depth estimates and bootstrap results; Table S3: Local adjacent-level constraints; Table S4: Deep convergence metrics; Table S5: Co-located horizontal-to-vertical convergence ratios; Table S6: Sensitivity of local crossing estimates to maximum plan-pairing distance.

**Author Contributions:** Conceptualisation, J.P., R.H. and A.A.M.; methodology, J.P., R.H. and A.A.M.; formal analysis, J.P.; investigation, D.K.; resources, D.K.; data curation, J.P. and D.K.; validation, D.K., R.H. and A.A.M.; visualisation, J.P.; writing—original draft preparation, J.P.; writing—review and editing, J.P., D.K., R.H. and A.A.M.; supervision, J.P., R.H. and A.A.M.; project administration, J.P. All authors have read and agreed to the published version of the manuscript.

**Funding:** This work was partly supported by the Polish Ministry of Science and Higher Education under grant DWD/6/0281/2022, by the "Excellence Initiative—Research University" programme at AGH University of Krakow, and by the AGH University of Krakow subsidy (grant 16.16.150.545; internal account 150000-501.00-10000).

**Institutional Review Board Statement:** Not applicable; this study did not involve humans or animals.

**Informed Consent Statement:** Not applicable.

**Data Availability Statement:** The detailed mine-monitoring data, exact monitoring coordinates, operational mine geometry, and integrated geodatabase cannot be made publicly available because they contain operationally sensitive information owned by the Salt Mine "Kłodawa" S.A. Sanitised aggregate data supporting the reported results, together with the core reproduction script, are supplied as Supplementary Materials. Additional non-sensitive extracts may be considered by the corresponding author upon reasonable request subject to approval by Salt Mine "Kłodawa" S.A.

**Acknowledgments:** The authors thank Salt Mine "Kłodawa" S.A. for providing access to the long-term surveying, mining, and geological records used in this study. During manuscript revision, OpenAI ChatGPT was used to support language editing, structural refinement, and non-substantive layout preparation. It was not used to generate or analyse study data, calculations, or scientific results. The authors verified all text, numerical values, and figures and take full responsibility for the final manuscript.

**Conflicts of Interest:** The authors declare no conflicts of interest. The funders had no role in the design of the study; in the collection, analysis, or interpretation of data; in the writing of the manuscript; or in the decision to publish the results.

## References

1. Senseny, P.E.; Hansen, F.D.; Russell, J.E.; Carter, N.L.; Handin, J.W. Mechanical behaviour of rock salt: Phenomenology and micromechanisms. *Int. J. Rock Mech. Min. Sci. Geomech. Abstr.* **1992**, *29*, 363–378. [CrossRef]
2. Munson, D.E. Constitutive model of creep in rock salt applied to underground room closure. *Int. J. Rock Mech. Min. Sci.* **1997**, *34*, 233–247. [CrossRef]
3. Cristescu, N.D. Non-associated elasto-viscoplastic models for rock salt. *Int. J. Eng. Sci.* **1999**, *37*, 269–297. [CrossRef]
4. Heusermann, S.; Rolfs, O.; Schmidt, U. Nonlinear finite-element analysis of solution mined storage caverns in rock salt using the LUBBY2 constitutive model. *Comput. Struct.* **2003**, *81*, 629–638. [CrossRef]
5. Hou, Z. Mechanical and hydraulic behavior of rock salt in the excavation disturbed zone around underground facilities. *Int. J. Rock Mech. Min. Sci.* **2003**, *40*, 725–738. [CrossRef]
6. Moghadam, S.N.; Nazokkar, K.; Chalaturnyk, R.J.; Mirzabozorg, H. Parametric assessment of salt cavern performance using a creep model describing dilatancy and failure. *Int. J. Rock Mech. Min. Sci.* **2015**, *79*, 250–267. [CrossRef]
7. Khaledi, K.; Mahmoudi, E.; Datcheva, M.; Schanz, T. Stability and serviceability of underground energy storage caverns in rock salt subjected to mechanical cyclic loading. *Int. J. Rock Mech. Min. Sci.* **2016**, *86*, 115–131. [CrossRef]
8. Reedlunn, B.; Argüello, J.G.; Hansen, F.D. A reinvestigation into Munson's model for room closure in bedded rock salt. *Int. J. Rock Mech. Min. Sci.* **2022**, *151*, 105007. [CrossRef]
9. Blanco-Martín, L.; Azabou, M.; Rouabhi, A.; Hadj-Hassen, F. Laboratory experiments on rock salt and phenomenological observations. *Int. J. Rock Mech. Min. Sci.* **2023**, *170*, 105452. [CrossRef]
10. Labaune, P.; Rouabhi, A.; Tijani, M.; Blanco-Martín, L.; You, T. Dilatancy criteria for salt cavern design: A comparison between stress- and strain-based approaches. *Rock Mech. Rock Eng.* **2018**, *51*, 599–611. [CrossRef]
11. Rouabhi, A.; Labaune, P.; Tijani, M.; Gatelier, N.; Hévin, G. Phenomenological behavior of rock salt: On the influence of laboratory conditions on the dilatancy onset. *J. Rock Mech. Geotech. Eng.* **2019**, *11*, 723–738. [CrossRef]
12. Modeste, G.; Masson, F.; Doubre, C.; Cornet, F.H. Repeated lidar acquisitions in an underground salt gallery in the Alsatian potassic basin (France): Monitoring and geomechanical modelling. *Tunn. Undergr. Space Technol.* **2022**, *123*, 104406. [CrossRef]
13. Furst, S.L.; Doucet, S.; Vernant, P.; Champollion, C.; Carme, J.-L. Monitoring surface deformation of deep salt mining in Vauvert (France), combining InSAR and leveling data for multi-source inversion. *Solid Earth* **2021**, *12*, 15–34. [CrossRef]
14. Barnhart, W.D.; Lohman, R.B. Regional trends in active diapirism revealed by mountain range-scale InSAR time series. *Geophys. Res. Lett.* **2012**, *39*, L08309. [CrossRef]
15. Szűcs, E.; Gönczy, S.; Bozsó, I.; Bányai, L.; Szakacs, A.; Szárnya, C.; Wesztergom, V. Evolution of surface deformation related to salt-extraction-caused sinkholes in Solotvyno (Ukraine) revealed by Sentinel-1 radar interferometry. *Nat. Hazards Earth Syst. Sci.* **2021**, *21*, 977–993. [CrossRef]
16. Pankratz, H.G.; Sultan, M.; Abdelmohsen, K.; Sauck, W.A.; Alsefry, S.; Alharbi, H.; Emil, M.K.; Gebremichael, E.; Asaeidi, A.; Alshehri, F.; et al. Use of geophysical and radar interferometric techniques to monitor land deformation associated with the Jazan salt diapir, Jazan City, Saudi Arabia. *Surv. Geophys.* **2021**, *42*, 177–200. [CrossRef]
17. Zhao, A.; Li, Y.; Shi, X.; Hao, S.; Che, Z.; Yang, K.; Xu, M.; Ma, H. Mechanism of anomalous "internal subsidence and peripheral uplift" in a salt mine goaf: A multi-source validated superposition of poroelastic uplift and mining-induced subsidence. *Geomech. Energy Environ.* **2025**, *44*, 100769. [CrossRef]
18. Burliga, S. Heterogeneity of folding in Zechstein (Upper Permian) salt formations in the Kłodawa Salt Structure, central Poland. *Geol. Q.* **2014**, *58*, 565–576. [CrossRef]
19. Kolano, M.; Cała, M.; Stopkowicz, A. Mechanical properties of rock salt from the Kłodawa salt dome—A statistical analysis of geomechanical data. *Materials* **2024**, *17*, 3564. [CrossRef] [PubMed]
20. Marcola-Sadowska, J.; Bieniasz, J.; Wojnar, W. Zaciskanie konturu typowej komory prostopadłościennej w Kopalni Soli Kłodawa [Convergence of the contour of a typical rectangular chamber in the Kłodawa Salt Mine]. *Geologia* **2009**, *35*, 307–314.

21. Bieniasz, J.; Wojnar, W.; Sadowski, A.; Wrzosek, J. Convergence of large depth mining excavations in salt rock formations. *Geol. Geophys. Environ.* **2011**, *37*, 207.
22. Kowalski, M.; Tajduś, A.; Cała, M.; Andrusikiewicz, W.; Kolano, M.; Stopkowicz, A.; Cyran, K.; Jakóbczyk, J. Long term analysis of deformations in salt mines: Kłodawa Salt Mine case study, central Poland. *Arch. Min. Sci.* **2017**, *62*, 565–577. [CrossRef]
23. Pietras, J.; Kurdek, D.; Malinowska, A.A. Monitoring the spatiotemporal deformation distribution in salt mines. In *Proceedings of the 24th International Multidisciplinary Scientific GeoConference SGEM 2024, Albena, Bulgaria, 29 June–8 July 2024*; SGEM: Vienna, Austria, 2024; Volume 24, pp. 221–228. [CrossRef]
24. Pietras, J.; Malinowska, A.A. Experimental validation of a laser distance measurement system for convergence monitoring in underground salt formations. *Meas. Sens.* **2026**, *46*, 102010. [CrossRef]
25. Khayrutdinov, M.M.; Ma, L.; Mangi, H.N.; Kongar-Syuryun, C.h.B.; Klyuev, R.V.; Petenko, A.; Brigida, V. Ensuring decarbonization underground construction technologies of backfilling based on the tailings. *Constr. Mater. Prod.* **2026**, *9*, 7. [CrossRef]
26. Weijermars, R.; Jackson, M.P.A.; Dooley, T.P. Quantifying drag on wellbore casings in moving salt sheets. *Geophys. J. Int.* **2014**, *198*, 965–977. [CrossRef]
27. Li, T.; Rui, Y.; Zhao, S.; Zhang, Y.; Zhu, H.; Li, X.; Lu, L. A quantitative digital twin maturity model for underground infrastructure based on D-ANP. *Tunn. Undergr. Space Technol.* **2024**, *146*, 105612. [CrossRef]
28. Babanagar, N.; Sheil, B.; Ninić, J.; Zhang, Q.; Hardy, S. Digital twins for urban underground space. *Tunn. Undergr. Space Technol.* **2025**, *155*, 106140. [CrossRef]
29. Adamuszek, M.; Tămaş, D.M.; Barabasch, J.; Urai, J.L. Rheological stratification in impure rock salt during long-term creep: Morphology, microstructure, and numerical models of multilayer folds in the Ocnele Mari salt mine, Romania. *Solid Earth* **2021**, *12*, 2041–2065. [CrossRef]
30. Bérest, P.; Brouard, B.; Feuga, B.; Karimi-Jafari, M. The 1873 collapse of the Saint-Maximilien panel at the Varangeville salt mine. *Int. J. Rock Mech. Min. Sci.* **2008**, *45*, 1025–1043. [CrossRef]
31. Bérest, P. Cases, causes and classifications of craters above salt caverns. *Int. J. Rock Mech. Min. Sci.* **2017**, *100*, 318–329. [CrossRef]
32. Li, X.; Tang, L.; Ling, J.; Chen, C.; Shen, Y.; Zhu, H. Digital-twin-enabled JIT design of rock tunnel: Methodology and application. *Tunn. Undergr. Space Technol.* **2023**, *140*, 105307. [CrossRef]
33. Machado, L.B.; Poncetti, B.L.; de Assis, L.S.; Futai, M.M. Automated procedural modeling for tunnel inspection and digital twin development. *Tunn. Undergr. Space Technol.* **2025**, *165*, 106929. [CrossRef]
34. Cui, Y.; Li, J.; Li, Y.; Zhang, Z.; Du, J. Multiscale geometric digital twins of mine tunnels that integrate topological evolution and local reconstruction. *Tunn. Undergr. Space Technol.* **2026**, *169*, 107317. [CrossRef]
35. Li, X.; Ye, L.; Bian, X. Sequential data assimilation for digital twin modeling of shield tunnel structure-soil interaction systems. *Tunn. Undergr. Space Technol.* **2026**, *168*, 107168. [CrossRef]


**Disclaimer/Publisher's Note:** The statements, opinions and data contained in all publications are solely those of the individual author(s) and contributor(s) and not of MDPI and/or the editor(s). MDPI and/or the editor(s) disclaim responsibility for any injury to people or property resulting from any ideas, methods, instructions or products referred to in the content.